N-(2,6-Dimethoxypyridine-3-yl)-9-Methylcarbazole-3-Sulfonamide as a Novel Tubulin Ligand against Human Cancer

Yue-Ming Wang,[1] Lai-Xing Hu,[1,3] Zhen-Ming Liu,[2] Xue-Fu You,[1] Sheng-Hua Zhang,[1] Jing-Rong Qu,[4] Zhuo-Rong Li,[1] Yan Li,[4] Wei-Jia Kong,[1] Hong-Wei He,[1] Rong-Guang Shao,[1] Liang-Ren Zhang,[4] Zong-Gen Peng,[1] David W. Boykin,[3] and Jian-Dong Jiang[1]

Abstract

Purpose: We have synthesized a new tubulin ligand *N*-(2,6-dimethoxypyridine-3-yl)-9-methylcarbazole-3-sulfonamide (IG-105). This work investigates its anticancer effect and mechanism.

Experimental Design: Anticancer efficacy was evaluated at the molecular target, cancer cells and nude mice. The mechanism was explored at submolecular, molecular, and cellular levels.

Results: IG-105 showed a potent activity against human leukemia and solid tumors in breast, liver, prostate, lung, skin, colon, and pancreas with IC_{50} values between 0.012 and 0.298 μmol/L. It was also active in drug-resistant tumor cells and not a P-glycoprotein substrate. It inhibited microtubule assembly followed by M-phase arrest, Bcl-2 inactivation, and then apoptosis through caspase pathways. The colchicine pocket on tubulin is the binding site of IG-105. Nude mice experiments showed that IG-105 monotherapy at 100 mg/kg i.p. (q2d) yielded 81% inhibition of Bel-7402 hepatoma growth and at 275 mg/kg i.p. (q2d) completely inhibited the tumor growth. MCF-7 breast cancer in nude mice showed a similar therapeutic response to IG-105. Acute toxicity of IG-105 was not found even at 1,000 mg/kg i.p. In combination with oxaliplatin or doxorubicin, IG-105 converted each of these subcurative compounds into a curative treatment with complete inhibition for tumor growth in the hepatoma-bearing nude mice. The combination was more active than either drug. In no experiment was toxicity increased by combination chemotherapy.

Conclusions: IG-105 inhibits microtubule assembly by binding at colchicine pocket. It shows a potent anticancer activity *in vitro* and *in vivo* and has good safety in mice. We consider IG-105 merits further investigation.

Microtubules are composed of α- and β-tubulin subunits. The major function of microtubules is to partition the duplicate chromosomes equally into the daughter cells through spindle formation during the mitosis of cell cycle (1, 2). In malignant cells, this process is essential for tumor growth and the dynamics of the tubulin-microtubule cycle speeds up in cell dividing (2–5). Tubulin-active agents block the microtubule assembly-disassembly dynamic and therefore kill tumor cells (6–8). They have shown significant therapeutic benefit in cancer patients (9). The representative drugs in clinic of such mode of action are *Vinca* alkaloids (such as vincristine) that inhibit microtubule assembly and Taxol analogues (such as paclitaxel) that disrupt the microtubules disassembly (10–12).

However, these drugs have major limitations. First, they have side effects in patients including neurologic toxicity and bone marrow suppression (13–16). Second, they are all substrates of P-glycoprotein (Pgp) and easy to induce multidrug resistance (17, 18). Chemically, they are all relatively big molecules isolated from plants with molecular weight of around 900 and therefore difficult for *de novo* synthesis. Searching for small-molecule tubulin ligands with novel chemical structure is an active research field; the goal is to discover new drug candidates with high efficacy against cancer and low toxicity *in vivo* (19).

Based on our background knowledge of α- and β-tubulin as well as its chemical ligands, over 450 compounds were designed and synthesized in our laboratories, in which a series of azaheterocyclic carbazole sulfonamides showed a promising antiproliferative activity in human cancer cell lines. The most potent compound was *N*-(2,6-dimethoxypyridine-3-yl)-9-methylcarbazole-3-sulfonamide (IG-105; ref. 20). We have then in the subsequent studies identified IG-105 as a new tubulin ligand with promising activity against cancer. Here, we report the molecular mechanism and *in vitro* activity of this compound. The anticancer efficacy of the compound in nude mice in monotherapy as well as combination therapy is also presented.

Authors' Affiliations: [1]Institute of Medicinal Biotechnology, Chinese Academy of Medical Sciences and Peking Union Medical College; [2]State Key Laboratory of Natural and Biomimetic Drugs, School of Pharmaceutical Sciences, Peking University, Beijing, People's Republic of China; [3]Department of Chemistry, Georgia State University, Atlanta, Georgia; and [4]Department of Medicine, Mount Sinai School of Medicine, New York, New York

Received 2/28/08; revised 5/20/08; accepted 5/22/08.

Grant support: National Natural Science Foundation of China grant 30371673 and Drug Discovery Program of the 11th 5-Y Plan of the Ministry of Science and Technology (J-D. Jiang).

The costs of publication of this article were defrayed in part by the payment of page charges. This article must therefore be hereby marked *advertisement* in accordance with 18 U.S.C. Section 1734 solely to indicate this fact.

Requests for reprints: Jian-Dong Jiang, Institute of Medicinal Biotechnology, Chinese Academy of Medical Sciences and Peking Union Medical College, 1 Tiantan Xili, Beijing 100050, People's Republic of China. Phone: 86-10-63165290; Fax: 86-10-63017302; E-mail: jiang.jdong@163.com or David W. Boykin, E-mail: dboykin@gsu.edu.

doi:10.1158/1078-0432.CCR-08-0550

Translational Relevance

The dynamic cycling between microtubule and tubulin represents a sensitive machinery to interrupt cancer cell dividing. Agents acting at the process, such as *Vinca* alkaloids and Taxol analogues, have been used as first-line drugs for cancer patients. However, current drugs in this category cause considerable side effects and drug resistance in clinical treatment. It is highly desirable to discover novel tubulin ligands that could avoid or minimize these problems. Our work focuses on the discovery of small molecular weight tubulin ligands. After a series of design, synthesis, and biological testing, we have identified a new tubulin ligand of *N*-(2,6-dimethoxypyridine-3-yl)-9-methylcarbazole-3-sulfonamide (IG-105), which showed a potent anticancer activity in a variety of human tumor cells *in vitro* and *in vivo*. We have illustrated the molecule mode of action of this compound and the mechanism of why IG-105 is active against drug-resistant cancer cells. Another important advantage of IG-105 is the low-toxicity feature showing a good safety in animals. Combination of IG-105 with known anticancer drugs largely improved the therapeutic efficacy. As a new generation of tubulin-active anticancer agent, IG-105 has been patented (PCT/CN2006/002298) and is now under preclinical evaluation.

Materials and Methods

Drugs and chemicals. IG-105 (molecular weight, 397; Fig. 1A) was synthesized in our laboratory with a purity over 98.5% (20). It was dissolved in DMSO at 10 mg/mL as a stock solution and further diluted in medium before each use. Colchicine, vincristine, paclitaxel, doxorubicin, oxaliplatin, and mitomycin C were purchased from Sigma. Z-DEVD-FMK (caspase-3 inhibitor), Z-IETD-FMK (caspase-8 inhibitor), and Z-LEHD-FMK (caspase-9 inhibitor) were obtained from R&D Systems.

Cell lines. Human tumor cell lines used in this study are listed in Table 1. The CEM, MIA PaCa-2, MCF-7, SW620, LoVo, DU-145, NCI-H23, and HUVEC cell lines were from the American Type Culture Collection. DND-1 and Molt-3 cell lines were kindly provided by Dr. Ohnuma (Mount Sinai School of Medicine). The human hepatoma cells Bel-7402 and SMMC-7721 were from the Cancer Institute, Chinese Academy of Medical Sciences. Pgp-overexpressing MCF-7/Dox/Pgp cells were kindly provided by Dr. Ling (Albert Einstein College of Medicine). The cell lines were cultured in RPMI 1640 (Invitrogen) supplemented with 10% fetal bovine serum, 100 units/mL penicillin, and 100 μg/mL streptomycin. All cultures were maintained in an incubator at 37°C with 5% CO_2 and humidified atmosphere.

Cytotoxicity assay. Cell viability was assessed with the 3-(4,5-dimethylthiazol-2-yl)-2,5-diphenyltetrazolium bromide assay (21). Cells were seeded into the 96-well microplates at 1×10^4 per well followed by IG-105 treatment at concentrations between 0 and 1 μmol/L for 72 h at 37°C. The supernatants were removed gently and cell viability was assessed. The plate was read in a microplate reader. The IC_{50} was determined in duplicates and each experiment was repeated at least three times under identical conditions. IC_{50} value was defined as the drug concentration that inhibits 50% cell growth compared with the untreated controls and calculated by regression analysis.

Pgp ATPase assay. Drug-stimulated activity of Pgp ATPase was detected by Pgp-Glo assay system (Promega). By following the user protocol provided by the vender, the activity of Pgp ATPase was measured in the presence or absence of 100 μmol/L Na_3VO_4, 200 μmol/L Verapamil (as a positive reference), 2 μmol/L vincristine, or 2 μmol/L IG-105. The luminescence of the sample reflects the ATP level in the sample, which is negatively correlated with the activity of Pgp ATPase and was detected in a luminometer (POLARstar Galaxy, BMG Labtech).

DNA fragmentation. Cellular DNA was extracted with a previously reported method (22) and then separated in a 2% agarose gel electrophoresis at 75 V for 2 h and the migration was visualized under UV light.

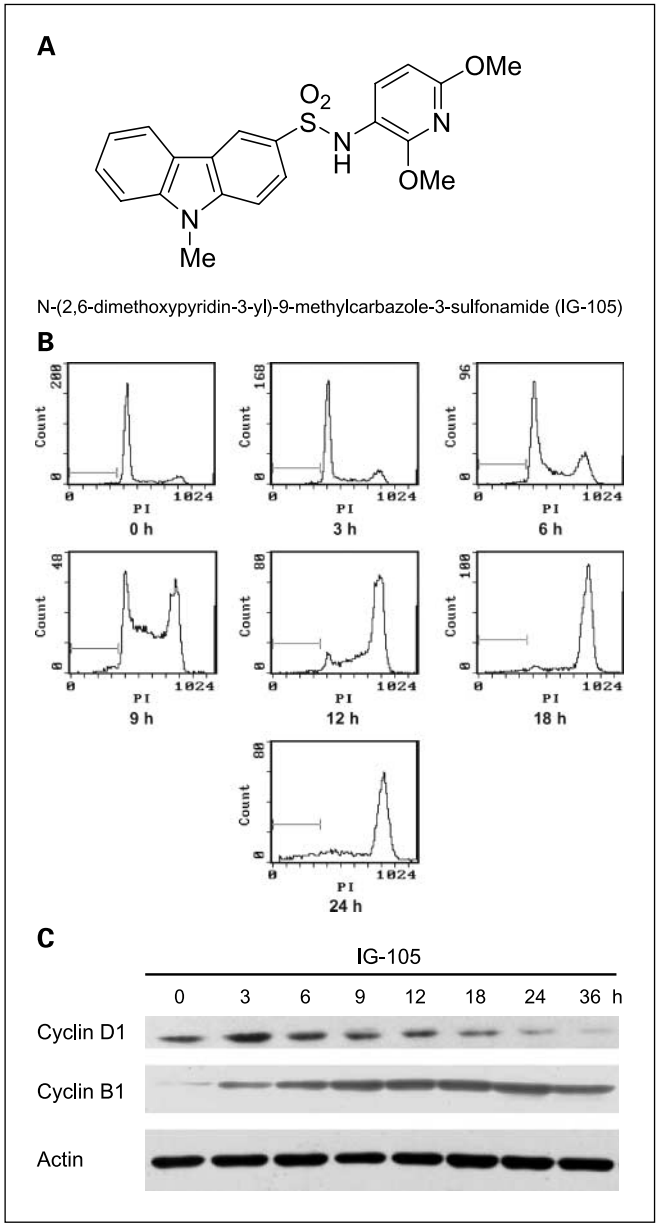

Fig. 1. Blockade of cell cycle at G_2-M phase in Bel-7402 cells treated with IG-105. *A,* chemical structure of IG-105. *B,* cell cycle analysis for Bel-7402 cells untreated (0 h) or treated with IG-105 at 0.35 μmol/L for 3, 6, 9, 12, 18, and 24 h. The majority of the cells were arrested at G_2-M phase after 9 h treatment. *C,* change of cyclins expression by IG-105. Bel-7402 cells were untreated (0 h) or treated with IG-105 (0.35 μmol/L) for 3, 6, 9, 12, 18, 24, and 36 h followed by protein extraction. Immunoblotting showed that cyclin B1 protein expression increased and cyclin D1 decreased after the treatment with IG-105.

Table 1. Cancericidal activity of IG-105 in the naive as well as resistant human tumor cell lines

(A) Anticancer spectrum

Cell line	Human tumor type	IC_{50} (μmol/L)
CEM	T-cell leukemia	0.133 ± 0.011
Molt-13	T-cell leukemia	0.158 ± 0.021
DND-1	Melanoma	0.012 ± 0.003
MIA PaCa-2	Pancreatic cancer	0.147 ± 0.023
MCF-7	Breast cancer	0.105 ± 0.007
Bel-7402	Hepatoma	0.173 ± 0.014
SW620	Colon cancer	0.249 ± 0.030
LoVo	Colon cancer	0.298 ± 0.024
DU-145	Prostate cancer	0.201 ± 0.020
NCI-H23	Lung cancer	0.274 ± 0.033
HUVEC	Nonmalignant	2.52 ± 0.43

(B) Cancericidal activity in the drug-resistant human cancer cells

Drug	IC_{50} (μmol/L)		Resistance index*	IC_{50} (μmol/L)		Resistance index
	Bel-7402	SMMC-7721		MCF-7	MCF-7/Dox/Pgp	
IG-105	0.179 ± 0.025	0.528 ± 0.126	3	0.151 ± 0.016	0.199 ± 0.08	1
Vincristine	0.059 ± 0.013	39.66 ± 1.68	672	0.006 ± 0.001	2.35 ± 0.56	391
Colchicine	0.008 ± 0.001	1.09 ± 0.12	132	0.013 ± 0.001	3.89 ± 0.38	300
Paclitaxel	0.025 ± 0.001	4.14 ± 0.53	165	0.003 ± 0.001	1.70 ± 0.58	566
Mitomycin C	1.346 ± 0.090	4.16 ± 0.03	3	0.159 ± 0.052	1.62 ± 0.77	10

(C) Drug effect on Pgp ATPase activity

Drug	Concentration (μmol/L)	Luminescence (relative light units)
Untreated	0	61,324 ± 1,200
Na_3VO_4	100	61,543 ± 1,037
Verapamil	200	51,210 ± 873 †
Vincristine	2	56,745 ± 979 †
IG-105	2	61,593 ± 2,253

NOTE: Mean ± SD of three independent experiments.
Relative light units represent the level of ATP in the sample, having a negative relationship with activity of Pgp ATPase. Na_3VO_4, negative control (not a substrate of Pgp); Verapamil, positive control (a substrate of Pgp); vincristine, a known drug reference.
*Resistance index is presented as a ratio of IC_{50} in the resistant cell line versus IC_{50} in the corresponding naive cell counterpart.
† $P < 0.01$, compared with the untreated group.

Cell cycle analysis. Cell cycle analysis was done with flow cytometry. Briefly, after drug treatment, cells were fixed in 70% ethanol overnight and then treated with RNase A and 50 μg/mL propidium iodide for 0.5 h at room temperature. Stained cell sample was immediately subjected to an analysis in a flow cytometer (Beckman Coulter). For each sample, 10,000 cells were counted and the cell cycle phase distribution was calculated using EPICS software (version 2.0).

Detection of caspase activation. The activities of the study caspases were measured with Caspase-Glo 3/7, Caspase-Glo 8, and Caspase-Glo 9 assay kits (Promega). Bel-7402 cells were treated with IG-105 at 0.35 μmol/L and harvested at different time points. The assays were done according to the user manual provided by the vender. The luminescence of the samples was measured in a luminometer (POLARstar Galaxy, BMG Labtech).

Tubulin polymerization assay. Tubulin polymerization was determined with the tubulin polymerization assay kit (Cytoskeleton) according to the vender's instructions. Tubulin polymerization dynamics was monitored through measuring the change of absorbance at 340 nm every 2 min for 30 min at 37°C on a spectrophotometer (Perkin-Elmer).

Immunofluorescence staining for microtubules structure. The microtubules structure in Bel-7402 cells treated with IG-105 was investigated using confocal microscopy. Paclitaxel and vincristine were used as positive controls. Bel-7402 cells attached to the coverslips were treated with 0.35 μmol/L IG-105, 0.5 μmol/L paclitaxel, or 0.1 μmol/L vincristine, respectively, for 12 h. The cells were fixed with 4% paraformaldehyde and blocked with 10% bovine serum albumin containing 0.1% Triton X-100. The cells were then stained with a FITC-conjugated α-tubulin monoclonal (Sigma) in a dilution of 1:200 for 2 h at 37°C. Then, the cells were treated with 4′,6-diamidino-2-phenylindole for 5 min. The stained cells were observed using a Leica TCS SP5 Confocal System (Leica Microsystems).

Molecular modeling and docking study. IG-105 was flexibly docked onto the colchicine binding site of α,β-tubulin crystal structure (PDB: 1SA0, tubulin in complex with DMA-colchicine; ref. 23) using AutoDock 3.05 program (24). Default variables were used as described in the AutoDock manual unless otherwise specified. The molecule was docked with 100 genetic algorithm runs of up to 250,000 energy evaluations for each run.

Scintillation proximity assay for the competition binding at tubulin. The colchicine and vinblastine scintillation proximity assays were conducted by following the instruction of the tubulin binding site competitive assay kit (Cytoskeleton). The reaction system contained [^{3}H]colchicine (Perkin-Elmer) or [^{3}H]vinblastine (GE) with final concentration of 0.16 or 0.64 μmol/L, test drugs, and biotin-labeled tubulin (1 μg) attached to yttrium streptavidin scintillation proximity assay beads (200 mg; GE). The reaction mixture was well mixed in 200 μL G-PEM buffer (80 mmol/L PIPES, 2 mmol/L $MgCl_2$, 1 mmol/L EGTA, and 0.1 mmol/L GTP) followed by incubation at 37°C for 30 min. Scintillation counting

was done on a MicroBeta Trilux Microplate scintillation counter (Perkin-Elmer Wallac).

Immunoblot analysis. Bel-7402 cells treated with IG-105 were collected. The protein extraction and immunoblot methods were described previously (25). Briefly, aliquots of cells were taken and lysed in radioimmunoprecipitation assay lysis buffer containing phenylmethylsulfonyl fluoride and protease inhibitor cocktail (Santa Cruz Biotechnology). Equal amount of lysate was subjected to a SDS-PAGE and then blotted onto the polyvinylidene difluoride membranes (Millipore) using a Semidry Electrophoretic Transfer System (Bio-Rad). Then, the membranes were blocked with 5% nonfat milk in TBST buffer (20 mmol/L Tris-HCl, 137 mmol/L NaCl, 0.05% Tween 20) at 37°C for 1 h and probed with mouse monoclonal antibodies against Bcl-2, Bax (Calbiochem), p53, p21, caspase-3, cyclin D1, and cyclin B1 (Santa Cruz Biotechnology), respectively, followed by incubation with goat anti-mouse antibody labeled with horseradish peroxidase. The signals were detected with enhanced chemiluminescence (Santa Cruz Biotechnology) and reserved after exposure to X-ray film.

Animal experiment. The inhibitory effect of IG-105 on human hepatoma Bel-7402 xenografts was examined in nude mice (female, ages 4-6 weeks, 18-20 g in weight) that were from the Institute of Experimental Animals, Chinese Academy of Medical Sciences. The mice received s.c. trocar grafts of Bel-7402 (6-8 mm^3/mouse, $\sim 10^7$ cells/mouse) on their backs. Ten days later, tumor-bearing mice were randomly divided into solvent control (untreated) and treatment cages with 6 mice per group. Drug treatment was initiated on day 11 post-implantation when the tumor volumes were between 170 and 200 mm^3. For the monotherapy, IG-105 was given at 100 or 275 mg/kg i.p. (q2d), oxaliplatin at 5 mg/kg i.p. (q2d), and doxorubicin at 1 mg/kg i.p. (q2d), respectively. For the combination therapy, IG-105 was administered at 175 mg/kg i.p. (q2d) in combination with oxaliplatin at 5 mg/kg i.p. (q2d) or doxorubicin at 1 mg/kg i.p. (q2d), respectively. Therapeutic response was monitored by measuring tumor volume three times a week until the tumor size in controls reached 2,000 mm^3, the criterion for euthanasia. Two perpendicular tumor diameters, width and length, were obtained with calipers and used to calculate tumor volume with the following formula: tumor volume = length $\times$ width^2 $\times$ 0.52 (25). The inhibition of tumor growth was calculated as follows: tumor growth inhibition rate (%) = $[(V_{c,end} - V_{c,start}) - (V_{d,end} - V_{d,start})] / (V_{c,end} - V_{c,start}) \times 100$, where $V_{c,start}$ is the average tumor volume of the untreated control in the beginning of therapy, $V_{c,end}$ is the average tumor volume of the untreated control at the end of therapy, $V_{d,start}$ is the average tumor volume of the drug-treated group in the beginning of therapy, and $V_{d,end}$ is the average tumor volume in drug-treated group at the end of therapy.

For the breast cancer model, 1×10^7 MCF-7 human breast cancer cells were injected s.c. into the mammary fat pad of the female nude mice. Estradiol pallets (1 mg/mouse) were implanted interscapularly 24 h before tumor implantation. Two weeks later, when the tumor grew to a volume around 200 mm^3, the mice were divided into four groups with 6 mice per each and were treated with saline (untreated control), paclitaxel (15 mg/kg i.p., q2d), or IG-105 (100 or 200 mg/kg i.p., q2d), respectively. Tumor volume was measured as described above.

Animal toxicity. Kunming mice (female, 18-20 g in weight) from the Institute of Experimental Animals, Chinese Academy of Medical Sciences were randomly divided into 6 groups with 6 mice per group. IG-105 was given i.p. at a single dose of 0, 400, 550, 700, 850, or 1,000 mg/kg, respectively. Body weight of the mice was followed up everyday for 15 days. Meanwhile, fur change, neurologic response, and behavior abnormality were closely monitored. Histopathologic examination was done for the major organs with H&E staining.

Results

Anticancer activity of IG-105 in human tumor cell lines. A wide range of cancer cell lines representing eight types of human tumor was examined (Table 1A). A variation of the sensitivity to IG-105 was observed among the cell lines with the IC_{50} ranged between 0.012 and 0.298 μmol/L. DND-1 melanoma cell line displayed the highest susceptibility with IC_{50} value of 0.012 μmol/L; in contrast, LoVo colon cancer cells and NCI-H23 lung cancer cells exhibited the lowest susceptibility to IG-105 with IC_{50} over 0.25 μmol/L. Between the two ends were the leukemia/lymphoma, hepatoma, breast cancer, pancreatic cancer and prostate cancer cells, from which we selected hepatoma for further studies as Chinese population has a high incidence of hepatoma. Non-malignant human HUVEC cells had an IC_{50} over 2.5 μmol/L in this experimental system.

Besides the Bel-7402 hepatoma cells, IG-105 was further tested in the SMMC-7721 hepatoma cells. This cell line is known to be resistant to tubulin-active anticancer drugs (such as vincristine and paclitaxel) but not to the DNA-damaging drugs (such as mitomycin C; ref. 26). The sensitivity of SMMC-7721 cells to vincristine or paclitaxel was much lower than that of Bel-7402 cells (Table 1B). However, IG-105 showed a potent cancericidal activity in either Bel-7402 or SMMC-7721 cells with a pattern similar to that of mitomycin C. The result suggests a unique activity of IG-105 in cancer cells resistant to tubulin-active drugs. To confirm the results, we also tested antiproliferative activity of IG-105 in the MCF-7/Dox/Pgp cells. IG-105 inhibited the growth of MCF-7/Dox/Pgp cells with an IC_{50} of 0.199 μmol/L, which was similar to that in the naive MCF-7 cells (Table 1B). In this cell line test, the resistance index of IG-105 was 1, whereas the resistance indices were between 300 and 566 for vincristine, colchicine, and paclitaxel. To learn whether IG-105 is a substrate of Pgp, its effect on Pgp ATPase activity was determined, as this enzyme is typically activated by the Pgp substrates for transportation. Unlike Verapamil and vincristine that caused a significant increase of the activity of Pgp ATPase ($P < 0.01$), IG-105 showed no stimulation of the Pgp ATPase activity (Table 1C). These results indicate that IG-105 is not a substrate of Pgp and provide an explanation for the activity of IG-105 in the MCF/Dox/Pgp cells.

Cell cycle arrest by IG-105. Exposure of Bel-7402 cells to IG-105 resulted in an accumulation of the cells in the G_2-M phase. As shown in Fig. 1B, untreated cells (0 h) showed a classic pattern of proliferating cells and proportionally distributed in the G_0-G_1 (72%), S (18%), and G_2-M (10%) phases. Treatment of the cells with IG-105 induced a major shift of the cells from the G_0-G_1 to the G_2-M phase; the G_2-M-phase peak elevated at 6 h of treatment and continuously mounted up at 24 h with 78% of the cells arrested in the G_2-M phase. Accordingly, the cell number at G_0-G_1 phase decreased, with only 4% in G_0-G_1 phase and 18% in S phase. Other cell lines (CEM and MCF-7) treated with IG-105 showed a similar response to the compound (data not shown).

The expression of cyclin B1 was then examined to biochemically validate the M-phase arrest by IG-105, as cyclin B1 is a known mitotic cyclin (27). Treatment of Bel-7402 cells with IG-105 resulted in an immediate time-dependent up-regulation of cyclin B1 (Fig. 1C); at the same time, the cyclin D1 (G_0-G_1 cyclin) level decreased (Fig. 1C). These results provide further evidence of M-phase blockage by IG-105 and are consistent with the morphologic change (chromosome spreading) in the cells treated with IG-105 (data not shown).

Inhibition of microtubule assembly by IG-105. We then tested whether IG-105 can directly affect microtubule assembly-

disassembly process in a cell-free system. As shown in Fig. 2A, IG-105 inhibited polymerization of tubulin in a concentration-dependent manner with an IC_{50} of 3 μmol/L. A complete inhibition of microtubule assembly was observed when the concentration of IG-105 was at 6 μmol/L. The inhibitory mechanism of IG-105 on microtubule dynamics was similar to that of vincristine but not paclitaxel, because it did not disrupt the disassembly of microtubules (data not shown).

Next, the effect of IG-105 on cellular microtubule network was explored using confocal microscopy. To visualize microtubules and chromosomal DNA, cells were stained with FITC-conjugated α-tubulin monoclonal antibody (green) and 4′,6-diamidino-2-phenylindole (blue). As shown in Fig. 2B, untreated control cells exhibited normal organization of microtubule network. Paclitaxel treatment resulted in an enhanced microtubule polymerization with increased density and formation of long thick microtubule bundles surrounding the nucleus (Fig. 2B). In contrast, vincristine caused a microtubule depolymerization characterized with destroyed filament-like structure, short microtubule fragments, and reduced microtubule density (Fig. 2B). IG-105 yielded a change similar to that of vincristine, showing short and curled microtubule fragments as well as reduced signal of microtubule network (Fig. 2B). The results were consistent with that in microtubule assembly experiment (Fig. 2A).

It was modeled in docking computation that the molecular conformation of IG-105 was notably close to the DMA-colchicine conformation within the binding site (Fig. 2C). The dimethoxypyridine moiety of IG-105 is buried well inside the β-tubulin hydrophobic pocket (pocket 2) containing Val-β238, Cys-β241, Leu-β242, Leu-β248, Ala-β250, Leu-β255, Ala-β317, Val-β318, and Ala-β354; it is similar to the action of trimethoxyphenyl moiety of DMA-colchicine (28). Meanwhile, the carbazole group of IG-105 occupies the hydrophobic pocket (pocket 1), which is constructed with the side chain of Thr-α179, Val-α181, Asn-β258, and Lys-β352. Unlike colchicine, the sulfoamino group of IG-105 provides a new hydrogen bond with Asp-β251 and the N atom of the carbazole group forms a hydrogen bond with Asn-β258.

To confirm that the colchicine pocket is the real biological binding site for IG-105 as predicted by the molecular modeling, the tubulin competition-binding scintillation proximity assay test was done in a cell-free system. As shown in Fig. 2D (*left*), IG-105 competitively inhibited the binding of [^{3}H]colchicine to the colchicine pocket on tubulin with an IC_{50} of 0.6 μmol/L, more potent than did colchicine itself (IC_{50}, 1 μmol/L). In

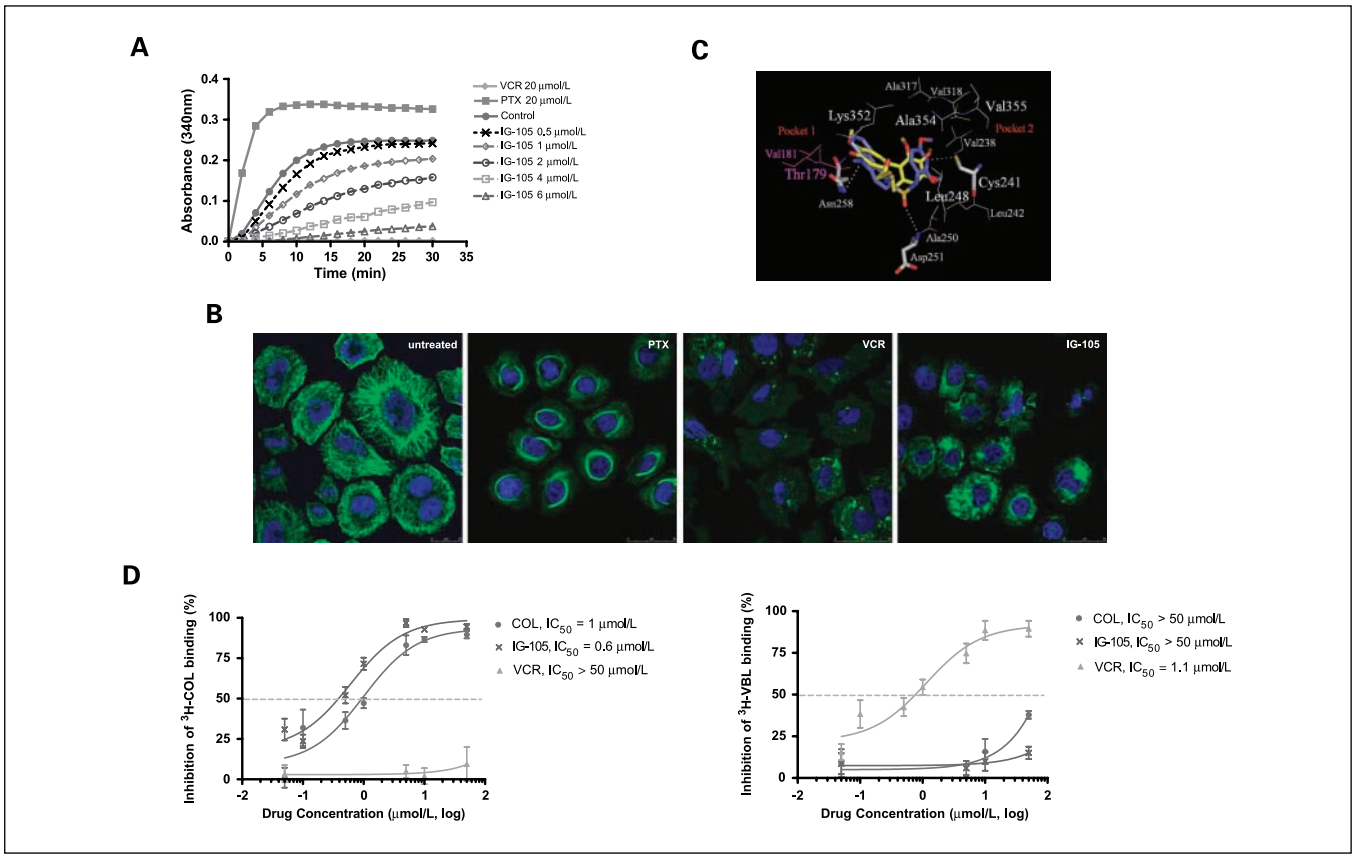

Fig. 2. Inhibitory effect of IG-105 on microtubule assembly. *A,* inhibitory effect of IG-105 on microtubule assembly. *In vitro* polymerization assay was done in the presence of IG-105, vincristine (*VCR*; 20 μmol/L), or paclitaxel (*PTX*; 20 μmol/L). *B,* disruption of the microtubule network by IG-105. The confocal micrographs display the change of microtubule network structure in Bel-7402 cells treated for 12 h with 0.5 μmol/L paclitaxel, 0.1 μmol/L vincristine, or 0.35 μmol/L IG-105, respectively (60 × 10). *C,* binding model of IG-105 at α,β-tubulin. IG-105 (*blue*) is bound to the interface between α-tubulin (*pink*) and β-tubulin (*white*) heterodimer, which overlaps with the DMA-colchicine (*yellow*) binding site in the tubulin crystal structure (1SA0). Hydrophobic pockets 1 and 2 are marked with the corresponding amino acid residues. Potential hydrogen bonds are shown in *dotted lines* (*white*). *D,* determination of the binding site of IG-105 on tubulin. Binding competition between IG-105 and [^{3}H]colchicine (*COL*) or [^{3}H]vinblastine (*VBL*) on tubulin was tested using the scintillation proximity assay test. The drug concentration is expressed in a log scale. *Points,* mean of three independent experiments; *bars,* SD.

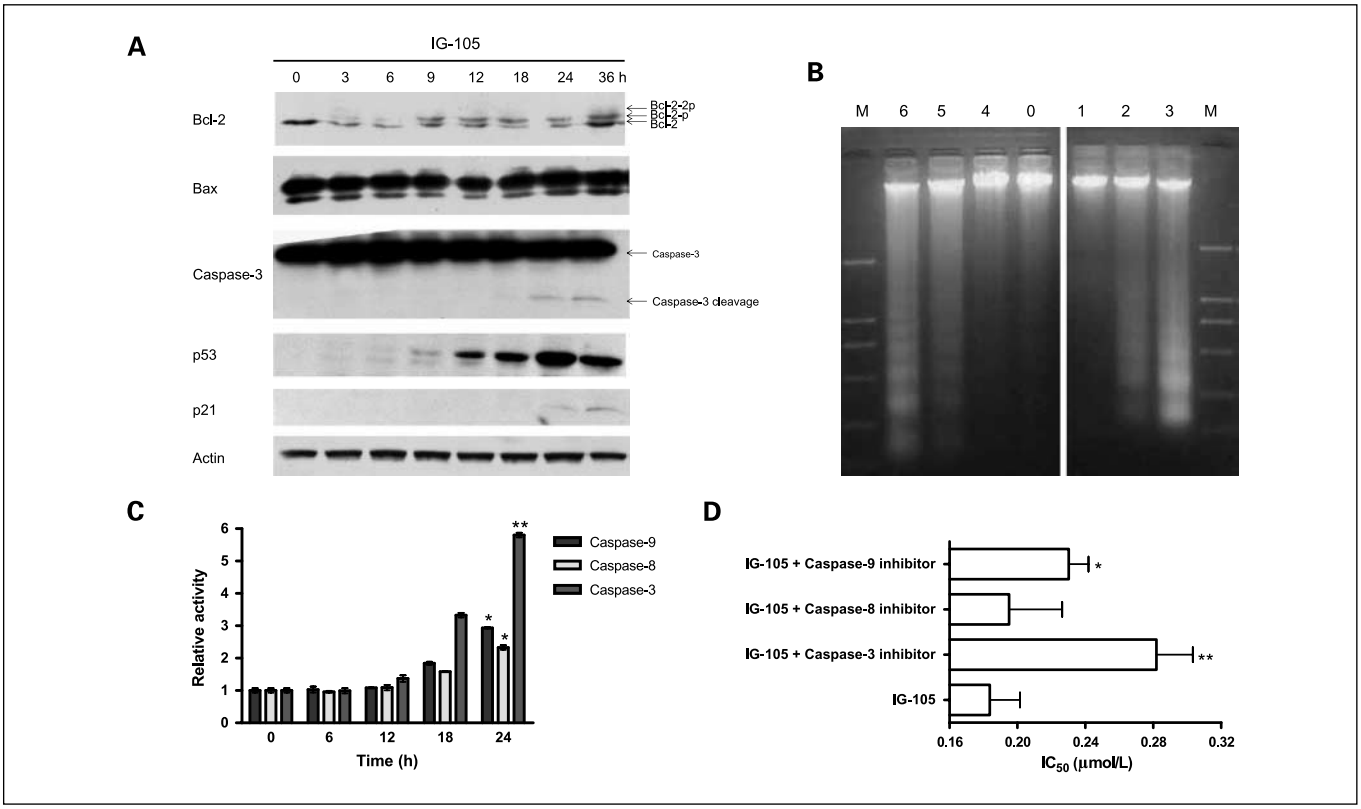

Fig. 3. Apoptosis induced by IG-105 in Bel-7402 cells. *A,* phosphorylation of Bcl-2, cleavage of caspase-3, and up-regulated p53 and p21 protein expression in Bel-7402 cells treated with IG-105 (0.35 μmol/L). *B,* DNA fragmented in Bel-7402 cells treated with IG-105. *Lane 0,* DNA from untreated Bel-7402 cells; *lanes 1* to *3,* DNA from cells treated with IG-105 for 48 h at the concentration of 0.086, 0.173, and 0.346 μmol/L, respectively; *lanes 4* to *6,* DNA from cells treated with IG-105 (0.35 μmol/L) for 12, 24, and 48 h, respectively; *lane M,* DNA marker (100-2,000 bp). *C,* IG-105-induced caspase activity. Activities of caspase-9, caspase-8, and caspase-3 in Bel-7402 cells increased after the treatment with IG-105 (0.35 μmol/L). *Columns,* mean of three independent experiments; *bars,* SD. *, $P < 0.05$; **, $P < 0.01$, compared with the corresponding 0 h group. *D,* pretreatment of Bel-7402 cells with caspase inhibitor reduced their sensitivity to IG-105. Pretreatment of Bel-7402 cells with 100 μmol/L caspase-3 inhibitor for 12 h partially abrogated the effect of IG-105; however, pretreatment with 100 μmol/L caspase-8 inhibitor or caspase-9 inhibitor shows less effect on the IC_{50} of IG-105. *Columns,* mean of three independent experiments; *bars,* SD. *, $P < 0.05$; **, $P < 0.01$, compared with the IG-105 group.

contrast, IG-105 did not compete with [^{3}H]vinblastine for its binding at the *Vinca* alkaloids binding site (Fig. 2D, *right*). These experiments strongly support the computer docking results described above.

Activation of apoptotic pathway by IG-105. Bcl-2 and Bax protein expression was analyzed with Western blot to learn the signal pathway of IG-105. Phosphorylated Bcl-2 in tumor cells became evident at 3 h after IG-105 treatment and increased with time, but the Bax expression remained unchanged (Fig. 3A). Cleavage of caspase-3 was found after 18 to 24 h on IG-105 treatment (Fig. 3A). Then, the apoptotic DNA, as a typical downstream event of caspase-3 pathway, appeared in the IG-105-treated cells (Fig. 3B).

The activities of caspase-3, caspase-8, and caspase-9 in the cells after IG-105 treatment were also detected (Fig. 3C). The intracellular activity of both caspase-8 and caspase-9 elevated by about 3-fold after 24 h exposure to IG-105, suggesting a cross-talk between caspase-8 and caspase-9 in the mechanism of IG-105. As the central apoptosis executioner, the activity of caspase-3 increased about 6-fold at 24 h. To confirm the role of the caspases in the cancericidal activity of IG-105, caspase inhibitors were used to pretreat the Bel-7402 cells before their exposure to IG-105. The abrogating effect was observed with caspase-3 inhibitor, which resulted in a 1.5-fold increase of the IC_{50} of IG-105 (Fig. 3D). Inhibition of caspase-8, or caspase-9, showed relatively minor effect on the IC_{50} of IG-105 (Fig. 3D).

IG-105 also caused a time-dependent up-regulation of p53 protein (Fig. 3A). The p21 expression was moderately affected by IG-105 but at later stage and after the elevation of p53 (Fig. 3A). The results are consistent with that of the known tubulin-active drugs (29).

Inhibition of tumor growth in nude mice. The drug treatment was started when the Bel-7402 tumor size in the nude mice was between 170 and 200 mm^3. On day 29 of the treatment, the average tumor volume in the solvent control was 2,049 ± 412 mm^3; however, the average tumor size was 518 ± 130 mm^3 in the group treated with low dose of IG-105 (100 mg/kg i.p., q2d), showing 81% inhibition of tumor volume, and was 183 ± 51 mm^3 in the high-dose IG-105 group (275 mg/kg i.p., q2d), showing a complete inhibition of tumor growth (Fig. 4A, *top*). No visible toxicity of IG-105 was observed during the treatment. The average body weight in the high-dose group remained stable with the starting point of 20.7 ± 0.7 g and the end point of 21.5 ± 0.8 g (Fig. 4A, *bottom*). Oxaliplatin (5 mg/kg i.p., q2d) and doxorubicin (1 mg/kg i.p., q2d) monotherapy inhibited the tumor volume by 57% and 60%, respectively, with no toxicity (Fig. 4A).

MCF-7 breast cancer showed a similar response to IG-105 *in vivo*. When the average tumor volume of the untreated control reached 2,380 ± 520 mm^3 on day 21 of the treatment, the average tumor size was 740 ± 140 mm^3 in the 100 mg/kg IG-105 group (i.p., q2d) and 337 ± 69 mm^3 in the 200 mg/kg IG-105 group (i.p., q2d), showing 76% and 93% inhibition of the tumor growth (Fig. 4B), respectively, with the body weight unchanged. Although paclitaxel at 15 mg/kg i.p. (q2d) controlled the tumor volume at 312 ± 96 mm^3 with a 94% inhibition of tumor growth as well (Fig. 4B), the treatment caused a loss of body weight from 22.3 ± 0.7 to 18.7 ± 0.7 g in average, indicating a toxicity of the regimen.

For the combination therapy (Fig. 4C and D), when the average tumor size of Bel-7402 hepatoma in the control group achieved 2,188 ± 517 mm^3 on day 31 of the treatment, the mean tumor size was 439 ± 49 mm^3 in the IG-105 monotherapy group (175 mg/kg i.p., q2d; 87% inhibition), 1,077 ± 338 mm^3 in the oxaliplatin group (5 mg/kg i.p., q2d; 55% inhibition), and 1,092 ± 359 mm^3 in the doxorubicin group (1 mg/kg i.p., q2d; 55% inhibition), respectively; however,

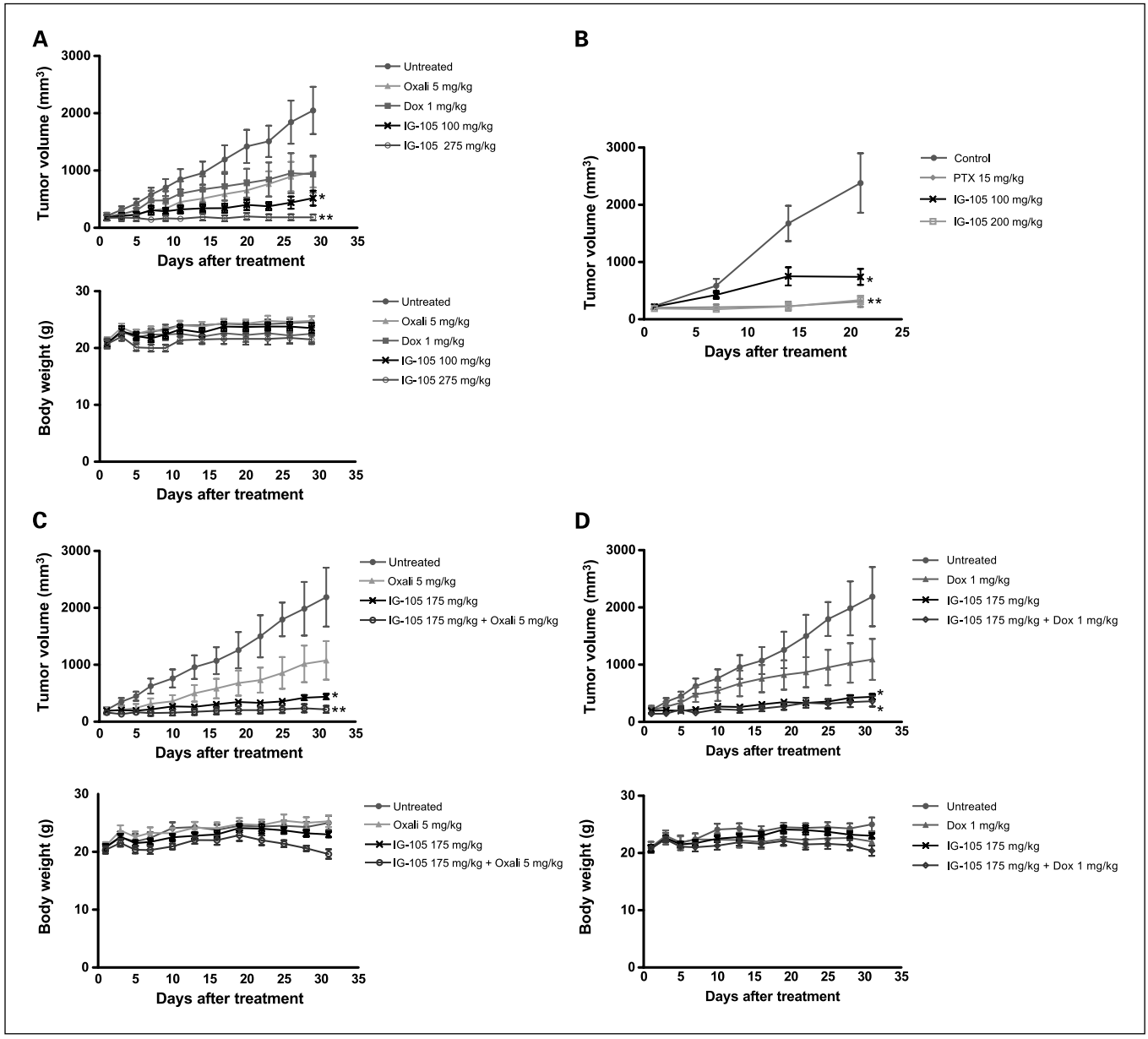

Fig. 4. Antitumor activity of IG-105 *in vivo*. *A,* anticancer efficacy of IG-105 (100 or 275 mg/kg i.p., q2d), oxaliplatin (5 mg/kg i.p., q2d), and doxorubicin (1 mg/kg i.p., q2d) against the Bel-7402 xenograft tumor in nude mice (*top*) and the body weight change during treatment (*bottom*). *Points,* mean of 6 mice in the group; *bars,* SE. *, $P < 0.05$; **, $P < 0.01$, compared with the untreated group. *B,* anticancer efficacy of IG-105 (100 or 200 mg/kg i.p., q2d) and paclitaxel (15 mg/kg i.p., q2d) against the MCF-7 xenograft tumor in nude mice. *Points,* mean of 6 mice in the group; *bars,* SE. *, $P < 0.05$; **, $P < 0.01$, compared with the untreated group. *C,* anticancer efficacy of the combination therapy using oxaliplatin (5 mg/kg i.p., q2d) and IG-105 (175 mg/kg i.p., q2d) against the Bel-7402 xenograft tumor in nude mouse (*top*) and the body weight change during treatment (*bottom*). *Points,* mean of 6 mice in the group; *bars,* SE. *, $P < 0.05$; **, $P < 0.01$, compared with the untreated group. *D,* anticancer efficacy of the combination therapy using doxorubicin (1 mg/kg i.p., q2d) and IG-105 (175 mg/kg i.p., q2d) against the Bel-7402 xenograft tumor in nude mice (*top*) and the body weight change during treatment (*bottom*). *Points,* mean of 6 mice in the group; *bars,* SE. *, $P < 0.05$, compared with the untreated group.

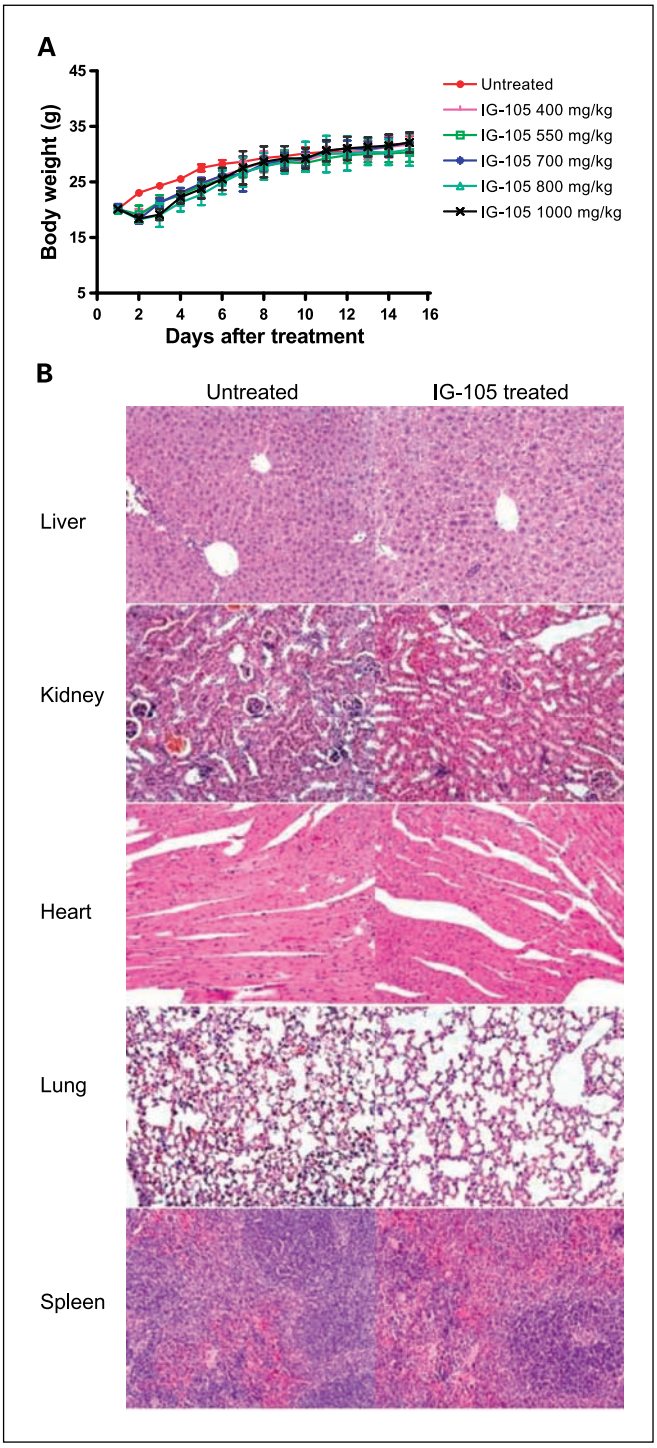

Fig. 5. Acute toxicity of IG-105 in mice. *A,* mouse body weight was monitored daily during IG-105 (i.p.) acute toxicity experiment in the healthy mice. *Points,* mean of 6 mice in the group; *bars,* SE. *B,* histopathologic examination (H&E) on liver, kidney, heart, lung, and spleen was done in the mice treated with IG-105 (1,000 mg/kg i.p.) at the end of acute toxicity experiment. No visible histopathologic changes were observed in these organs (20 × 10).

the tumor size was only 217 ± 61 mm^3 in the group combining IG-105 with oxaliplatin (complete inhibition; Fig. 4C, *top*) and 360 ± 93 mm^3 in the mice treated with IG-105 in combination with doxorubicin (89% inhibition; Fig. 4D, *top*). There was no evidence of toxicity of the regimen based on the measurement of survival and body weight (Fig. 4C and D, *bottom*).

Safety profile in normal mice. The acute toxicity of IG-105 (i.p.) was examined in healthy mice. IG-105 did not cause death and body weight loss even when the dose of the compound went up to 1,000 mg/kg (Fig. 5A), showing a good safety of the compound *in vivo*. Fur change and behavior abnormality were not observed. The results agreed with that in tumor-bearing nude mice. At the end of the study (on day 15), histologic examination (H&E) of the mice organs showed no evidence of pathologic damage in liver, kidney, heart, lung, and spleen (Fig. 5B).

Discussion

IG-105 is a novel synthetic tubulin ligand with small molecular weight. The primary action of IG-105 in cancer cells is to inhibit microtubule assembly, similar to that of *Vinca* alkaloids. The binding site of IG-105 on tubulin appears to be the colchicine pocket. The disruption of microtubules by IG-105 leads to the activation of Checkpoint 2, which causes the accumulation of cells at M phase (14, 30). This observation was supported by the accumulation of cyclin B1 in the cells treated with IG-105, as cyclin B1 must be degraded into the inactivate M-phase-promoting factor for the cells to exit from mitosis and enter into the next interphase (31, 32). Cyclin B1 degradation appeared to be abolished in the IG-105-treated cells. Presently, there is one established mechanism that is known to communicate between mitotic arrest and apoptosis (33), in which Bcl-2 is a key factor. Bcl-2 is a mitochondria integral membrane protein that functions as an apoptosis suppressor though formation of heterodimer with Bax, an apoptosis enhancer (34, 35). Phosphorylation of Bcl-2 inactivates Bcl-2 and makes it incapable of forming heterodimers with Bax. It therefore alters the intracellular balance between Bcl-2 and Bax, driving the Bcl-2-positive cells into an apoptotic cascade. This process has been reported as a feature of the signal pathway for the tubulin-active agents such as *Vinca* alkaloids and paclitaxel (36–38). The results obtained with IG-105 fit the pathway well. The M-phase peak began to rise at 3 to 6 h after IG-105 treatment. The earliest visible Bcl-2 phosphorylation occurred also between 3 and 6 h, which is a known trigger of the caspases (39–41). Both caspase-8 and capsase-9 were activated in the tumor cells treated with IG-105, indicating a cross-talk between the two cascades (42) in the IG-105 mechanism. Subsequently, the caspase-3 was cleaved and the activity was enhanced by 6-fold at 24 h. The visible fragmented DNA appeared after 24 h of treatment. The expression of p53 increased after Bcl-2 inactivation, indicating a secondary mechanism of apoptosis (43) in the IG-105-treated cells. The enhanced cytoplasmic p53 might also abolish the activity of Bcl-2 (44). This phenomenon has also been reported in paclitaxel-treated cancer cells (45).

Different from vincristine, IG-105 showed a strong cancericidal activity in human hepatoma SMMC-7721 cells, a tubulin-active drug-resistant cell line with the mechanism unknown (46). The anticancer efficacy of IG-105 in SMMC-7721 cells was comparable with its activity in Bel-7402 cells and similar to that of DNA-targeting agent mitomycin C. Similarly, the killing effect of IG-105 on MCF-7 cells with or without Pgp was

identical, further supporting its activity in drug-resistant tumor cells. This feature makes IG-105 unique among anticancer tubulin ligands. There could be several explanations. First, IG-105 triggers either Bcl-2- or p53- related pathways, as SMMC-7721 is sensitive to DNA-targeting anticancer agents that cause p53 up-regulation. Second, IG-105 acts at the colchicine binding pocket on tubulin different from that of *Vinca* alkaloids. Third, IG-105 is not a substrate of Pgp.

One of the most impressive effects of IG-105 is its potent anticancer effect *in vivo*. IG-105 monotherapy generated a complete inhibition of tumor growth in human hepatoma and 93% inhibition in breast cancer at nontoxic dose. High dose of IG-105 was more effective than the low one did, compatible with the theory that high-dose chemotherapy might be potentially curative for certain types of cancer. The therapeutic efficacy of IG-105 was much greater than that of vincristine as well as the small-molecule tubulin ligands we reported before (25, 46). The effectiveness of IG-105 in animals also hints a favorable bioavailability of the compound *in vivo*. As it is still pioneer experiments in animals, modification of the treatment regimen might improve the higher therapeutic efficacy. Another important feature of the compound is the low toxicity in animals. All of the mice survived with no change of their body weight even when the dose of IG-105 was as high as 1,000 mg/kg i.p. Pathologic examination showed no damage on liver, kidney, heart, lung, and spleen after the mice received 1,000 mg/kg IG-105. It provides a substantial advantage of the compound with respect to other tubulin ligands. Specific binding at the colchicine pocket on tubulin with a high affinity could be part of the explanation. As the ED_{50} of IG-105 in Bel-7402 hepatoma was about 50 to 70 mg/kg in the present study, the therapeutic index of IG-105 fell into an arrange between 15 and 20, higher than that of vincristine (25).

In the animal experiments, we have combined IG-105 with DNA-interactive drug oxaliplatin and topoisomerase-2 inhibitor doxorubicin. The two drugs were selected because they are used in patients with hepatoma and their mechanisms are independent of microtubules. Bel-7402 hepatoma showed a complete growth inhibition to the combination therapy using IG-105 with oxaliplatin, indicating a conversion of the subcurative dose of oxaliplatin into a curative treatment by IG-105 for human hepatoma in nude mice. The anticancer effect of IG-105 in combination with oxaliplatin was synergistic, and it could be explained by the cooperation of the multiple mechanisms. Toxicity of the combination was not observed in either of the regimen.

Future anticancer drug development has been focused on new mechanism drug molecules with increased potency, effectiveness on drug-resistant cancers, and decreased side effects. We consider IG-105 fills the need.

Disclosure of Potential Conflicts of Interest

No potential conflicts of interest were disclosed.

References

1. Jordan MA, Wilson L. Microtubules as a target for anticancer drugs. Nat Rev Cancer 2004;4:253–65.
2. Desai A, Mitchison TJ. Microtubule polymerization dynamics. Annu Rev Cell Dev Biol 1997;13:83–117.
3. Brangwynne CP, MacKintosh FC, Weitz DA. Force fluctuations and polymerization dynamics of intracellular microtubules. Proc Natl Acad Sci U S A 2007; 104:16128–33.
4. Howard J, Hyman AA. Dynamics and mechanics of the microtubule plus end. Nature 2003;422:753–8.
5. Rusan NM, Fagerstrom CJ, Yvon AM, Wadsworth P. Cell cycle-dependent changes in microtubule dynamics in living cells expressing green fluorescent protein-α tubulin. Mol Biol Cell 2001;12:971–80.
6. Jordan MA, Thrower D, Wilson L. Mechanism of inhibition of cell proliferation by *Vinca* alkaloids. Cancer Res 1991;51:2212–22.
7. Yvon AM, Wadsworth P, Jordan MA. Taxol suppresses dynamics of individual microtubules in living human tumor cells. Mol Biol Cell 1999;10:947–59.
8. Wilson L, Panda D, Jordan MA. Modulation of microtubule dynamics by drugs: a paradigm for the actions of cellular regulators. Cell Struct Funct 1999; 24:329–35.
9. Bhalla KN. Microtubule-targeted anticancer agents and apoptosis. Oncogene 2003;22:9075–86.
10. Jackson JR, Patrick DR, Dar MM, Huang PS. Targeted anti-mitotic therapies: can we improve on tubulin agents? Nat Rev Cancer 2007;7:107–17.
11. Mollinedo F, Gajate C. Microtubules, microtubule-interfering agents and apoptosis. Apoptosis 2003;8: 413–50.
12. Openshaw H, Beamon K, Synold TW, et al. Neurophysiological study of peripheral neuropathy after high-dose paclitaxel: lack of neuroprotective effect of amifostine. Clin Cancer Res 2004;10:461–7.
13. Schmidt M, Bastians H. Mitotic drug targets and the development of novel anti-mitotic anticancer drugs. Drug Resist Updat 2007;10:162–81.
14. Tao W, South VJ, Zhang Y, et al. Induction of apoptosis by an inhibitor of the mitotic kinesin KSP requires both activation of the spindle assembly checkpoint and mitotic slippage. Cancer Cell 2005;8:49–59.
15. Lee JJ, Low JA, Croarkin E, et al. Changes in neurologic function tests may predict neurotoxicity caused by ixabepilone. J Clin Oncol 2006;24:2084–91.
16. Sampath D, Greenberger LM, Beyer C, et al. Preclinical pharmacologic evaluation of MST-997, an orally active taxane with superior *in vitro* and *in vivo* efficacy in paclitaxel- and docetaxel-resistant tumor models. Clin Cancer Res 2006;12:3459–69.
17. Dumontet C, Sikic BI. Mechanisms of action of and resistance to antitubulin agents: microtubule dynamics, drug transport, and cell death. J Clin Oncol 1999; 17:1061–70.
18. Gururaja TL, Goff D, Kinoshita T, et al. R-253 disrupts microtubule networks in multiple tumor cell lines. Clin Cancer Res 2006;12:3831–42.
19. Giannakakou P, Sackett D, Fojo T. Tubulin/microtubules: still a promising target for new chemotherapeutic agents. J Natl Cancer Inst 2000;92:182–3.
20. Hu L, Li ZR, Wang YM, Wu Y, Jiang JD, Boykin DW. Novel pyridinyl and pyrimidinylcarbazole sulfonamides as antiproliferative agents. Bioorg Med Chem Lett 2007;17:1193–6.
21. Rubinstein LV, Shoemaker RH, Paull KD, et al. Comparison of *in vitro* anticancer-drug-screening data generated with a tetrazolium assay versus a protein assay against a diverse panel of human tumor cell lines. J Natl Cancer Inst 1990;82:1113–8.
22. Jiang JD, Wang Y, Roboz J, Strauchen J, Holland JF, Bekesi JG. Inhibition of microtubule assembly in tumor cells by 3-bromoacetylamino benzoylurea, a new cancericidal compound. Cancer Res 1998;58: 2126–33.
23. Ravelli RB, Gigant B, Curmi PA, et al. Insight into tubulin regulation from a complex with colchicine and a stathmin-like domain. Nature 2004;428:198–202.
24. Morris GM, Goodsell DS, Halliday RS, et al. Automated docking using a Lamarckian genetic algorithm and an empirical binding free energy function. J Comput Chem 1998;19:1639–62.
25. Jiang JD, Denner L, Ling YH, et al. Double blockade of cell cycle at G_1-S transition and M phase by 3-iodoacetamido benzoyl ethyl ester, a new type of tubulin ligand. Cancer Res 2002;62:6080–8.
26. Huang YH, Shang BY, Zhen YS. Antitumor efficacy of lidamycin on hepatoma and active moiety of its molecule. World J Gastroenterol 2005;11:3980–4.
27. Nurse P. Universal control mechanism regulating onset of M-phase. Nature 1990;344:503–8.
28. Mooberry SL, Weiderhold KN, Dakshanamurthy S, et al. Identification and characterization of a new tubulin-binding tetrasubstituted brominated pyrrole. Mol Pharmacol 2007;72:132–40.
29. Tishler RB, Lamppu DM, Park S, Price BD. Microtubule-active drugs Taxol, vinblastine, and nocodazole increase the levels of transcriptionally active p53. Cancer Res 1995;55:6021–5.
30. Kops GJ, Weaver BA, Cleveland DW. On the road to cancer: aneuploidy and the mitotic checkpoint. Nat Rev Cancer 2005;5:773–85.
31. Chang DC, Xu N, Luo KQ. Degradation of cyclin B is required for the onset of anaphase in mammalian cells. J Biol Chem 2003;278:37865–73.
32. Wasch R, Engelbert D. Anaphase-promoting complex-dependent proteolysis of cell cycle regulators and genomic instability of cancer cells. Oncogene 2005;24:1–10.
33. Weaver BA, Cleveland DW. Decoding the links between mitosis, cancer, and chemotherapy: the mitotic checkpoint, adaptation, and cell death. Cancer Cell 2005;8:7–12.
34. Cory S, Adams JM. Killing cancer cells by flipping the Bcl-2/Bax switch. Cancer Cell 2005;8:5–6.
35. Green DR, Kroemer G. The pathophysiology of mitochondrial cell death. Science 2004;305:626–9.

36. Fan M, Du L, Stone AA, Gilbert KM, Chambers TC. Modulation of mitogen-activated protein kinases and phosphorylation of Bcl-2 by vinblastine represent persistent forms of normal fluctuations at G2-1. Cancer Res 2000;60:6403–7.

37. Mhaidat NM, Zhang XD, Jiang CC, Hersey P. Docetaxel-induced apoptosis of human melanoma is mediated by activation of c-Jun NH_2-terminal kinase and inhibited by the mitogen-activated protein kinase extracellular signal-regulated kinase 1/2 pathway. Clin Cancer Res 2007;13:1308–14.

38. Haldar S, Chintapalli J, Croce CM. Taxol induces bcl-2 phosphorylation and death of prostate cancer cells. Cancer Res 1996;56:1253–5.

39. Danial NN, Korsmeyer SJ. Cell death: critical control points. Cell 2004;116:205–19.

40. Kroemer G, Martin SJ. Caspase-independent cell death. Nat Med 2005;11:725–30.

41. Sun XM, MacFarlane M, Zhuang J, Wolf BB, Green DR, Cohen GM. Distinct caspase cascades are initiated in receptor-mediated and chemical-induced apoptosis. J Biol Chem 1999;274:5053–60.

42. Basu A, Castle VP, Bouziane M, Bhalla K, Haldar S. Crosstalk between extrinsic and intrinsic cell death pathways in pancreatic cancer: synergistic action of estrogen metabolite and ligands of death receptor family. Cancer Res 2006;66:4309–18.

43. Vogel C, Kienitz A, Hofmann I, Muller R, Bastians H. Crosstalk of the mitotic spindle assembly checkpoint with p53 to prevent polyploidy. Oncogene 2004;23:6845–53.

44. Perfettini JL, Kroemer RT, Kroemer G. Fatal liaisons of p53 with Bax and Bak. Nat Cell Biol 2004;6:386–8.

45. Giannakakou P, Robey R, Fojo T, Blagosklonny MV. Low concentrations of paclitaxel induce cell type-dependent p53, p21 and G_1/G_2 arrest instead of mitotic arrest: molecular determinants of paclitaxel-induced cytotoxicity. Oncogene 2001;20:3806–13.

46. Li JN, Song DQ, Lin YH, et al. Inhibition of microtubule polymerization by 3-bromopropionylamino benzoylurea (JIMB01), a new cancericidal tubulin ligand. Biochem Pharmacol 2003;65:1691–9.